Phenotypic and Functional Alterations in Tunneling Nanotubes Formed by Glaucomatous Trabecular Meshwork Cells

Ying Ying Sun, John M. Bradley, and Kate E. Keller

Casey Eye Institute, Oregon Health & Science University, Portland, Oregon, United States

Correspondence: Kate E. Keller, Casey Eye Institute, Oregon Health & Science University, 3181 SW Sam Jackson Park Road, Portland, OR 97239, USA; gregorka@ohsu.edu.

Submitted: July 25, 2019
Accepted: September 25, 2019

Citation: Sun YY, Bradley JM, Keller KE. Phenotypic and functional alterations in tunneling nanotubes formed by glaucomatous trabecular meshwork cells. *Invest Ophthalmol Vis Sci*. 2019;60:4583–4595. https://doi.org/10.1167/iovs.19-28084

Purpose. Trabecular meshwork (TM) cells detect and coordinate responses to intraocular pressure (IOP) in the eye. TM cells become dysfunctional in glaucoma where IOP is often elevated. Recently, we showed that normal TM (NTM) cells communicate by forming tubular connections called tunneling nanotubes (TNTs). Here, we investigated TNTs in glaucomatous TM (GTM) cells.

Methods. Primary GTM and NTM cells were established from cadaver eyes. Transfer of Vybrant DiO and DiD-labeled vesicles via TNT connections was measured. Imaris software measured the number and length of cell protrusions from immunofluorescent confocal images. Live-cell imaging of the actin cytoskeleton was performed. The distribution of myosin-X, a regulator of TNTs/filopodia, was investigated in TM cells and tissue.

Results. GTM cells contained significantly more transferred fluorescent vesicles than NTM cells (49.6% vs. 35%). Although NTM cells had more protrusions at the cell surface than GTM cells (7.61 vs. 4.65 protrusions/cell), GTM protrusions were significantly longer (12.1 μm vs. 9.76 μm). Live-cell imaging demonstrated that the GTM actin cytoskeleton was less dynamic, and vesicle transfer between cells was significantly slower than NTM cells. Furthermore, rearrangement of the actin cortex adjacent to the TNT may influence TNT formation. Myosin-X immunostaining was punctate and disorganized in GTM cells and tissue compared to age-matched NTM controls.

Conclusions. Together, our data demonstrate that GTM cells have phenotypic and functional differences in their TNTs. Significantly slower vesicle transfer via TNTs in GTM cells may delay the timely propagation of cellular signals when pressures become elevated in glaucoma.

Keywords: glaucoma, trabecular meshwork, actin cytoskeleton, filopodia, tunneling nanotube, myosin-X

Tunneling nanotubes (TNTs) are a novel method of cellular communication that allow the direct transfer of signals and organelles from cell to cell.[1–3] TNTs are a specialized type of filopodia. They were first described by Rustom et al.[4] in rat pheochromocytoma PC12 cells, but subsequent studies have detected them in many other cell types.[5–9] Two methods of TNT formation have been proposed: an "actin-driven" model, where filopodia tips extending from adjacent cells fuse to form a hollow connection through which cargo can travel; and a "cell dislodgement" model, where cells fuse and a thin tube is drawn out between cells as they move away from each other.[3,4,10]

Several molecules are involved in TNT formation, including myosin-X (Myo10), an unconventional myosin that is involved in both filopodia and TNT formation.[11–14] Myo10 is comprised of a myosin head domain that binds to actin filaments and a tail domain of the protein, which binds and transports cargo to filopodia tips.[15,16] Myo10 is also localized to podosomes and podosome-like structures, which function as both cell attachment sites as well as areas of focal extracellular matrix degradation.[17,18] Myo10 appears to position podosomes in a cell by linking actin and microtubule networks.[17] Importantly, Myo10 is also involved in filopodia and TNT formation.[12,13] The overall number of filopodia at the cell surface and filopodia length were reduced by silencing Myo10 or by using CK-666, an Arp2/3 inhibitor that blocks assembly of branched actin networks from which filopodia arise.[19–21] In addition, CK-666 treatment negatively affected the transfer of vesicles in TM cells.[20] Thus, there appears to be a correlation between Myo10 expression, the number and length of filopodia, and vesicle transfer via TNTs.

Evidence is mounting that TNTs play a role in pathologic disease. For instance, TNTs are involved in several neurodegenerative diseases, such as Parkinson's, Alzheimer's, and Huntington's, as well as in cancer and in the spread of prions, human immunodeficiency virus, and other pathogens.[2,22–25] Moreover, upregulation of Myo10 appears to influence breast cancer metastases.[26] Glaucoma is a group of neurodegenerative diseases that cause irreversible blindness.[27] Elevated intraocular pressure (IOP) is a common feature of the disease. Trabecular meshwork (TM) cells in the anterior chamber sense IOP elevations and communicate signals to coordinate focal extracellular matrix remodeling to allow greater aqueous humor outflow, thereby lowering IOP.[28,29] The TM cell actin cytoskeleton also has a role in IOP regulation. Reducing actin stress fibers by Rho-ROCK inhibition, or latrunculin-B admin-

istration, can facilitate aqueous outflow, thereby alleviating elevated IOP.[30–33] Previous studies showed that TM cells derived from human cadaver glaucoma eyes retain some of the abnormal in vivo characteristics when placed in culture. For instance, glaucomatous TM (GTM) cells synthesized altered extracellular matrices, had dysregulated autophagy, and assembled different actin cytoskeleton networks than normal TM (NTM) cells.[34–37]

Using live-cell imaging of TM cells, we recently demonstrated that cellular vesicles and mitochondria transferred via TNTs between TM cells in culture.[20] However, it is unknown whether TM cells derived from glaucoma patients form TNTs. Here, we compared TNT-mediated vesicle transfer, actin dynamics, and Myo10 distribution in normal and glaucomatous cells and tissue to investigate the role of TNTs in glaucoma.

Materials and Methods

Primary TM Cell Culture

Primary human TM cells were established from normal (NTM) and glaucomatous (GTM) cadaver eyes following published guidelines.[38] Experiments using human cadaver tissue were conducted in accordance with the tenets of the Declaration of Helsinki. Demographic data for the human cadaver eyes are in Supplementary Table S1. All cell strains were split 1:3 and used up to a maximum of six passages.

Western Immunoblotting and Densitometry

Myocilin induction of GTM cells by dexamethasone was performed as described previously.[18] The same publication shows myocilin induction by NTM cells used in this study. For Myo10 immunoblots, a rabbit polyclonal myosin-X primary antibody (PA5-55019; ThermoFisher, Waltham, MA, USA) and an IRDye 700-conjugated anti-rabbit secondary antibody were used. Membranes were scanned using an Odyssey gel imaging system (Licor, Lincoln, NE, USA). The intensity of the expected 260-kDa band was quantitated from each lane using ImageJ software. Also, myocilin immunostaining of GTM and NTM cells in culture was performed with and without dexamethasone treatment for 7 days. The immunostaining protocol is detailed below.

Phagocytosis Assay

Phagocytosis was measured as described previously.[18] Briefly, 100-µL opsonized pHrodo *Staphylococcus aureus* bioparticles (ThermoFisher) were added to each well of a 6-well plate containing GTM or NTM cells. The plate was placed in the Incucyte ZOOM instrument (Essen Bioscience, Ann Arbor, MI, USA), and each well was imaged every 15 minutes for 18 hours by using the phase and red fluorescence channels. Fluorescence at each time point was measured using open-source FIJI software (http://fiji.sc/Fiji). Data are from three technical replicates of >3 GTM and NTM cell strains.

Cellular Senescence Assay

Cellular senescence was measured using a β-galactosidase staining kit (Cell Signaling Technologies, Danvers, MA, USA) following the manufacturer's directions. Images were acquired using a BX51 microscope (Olympus, Waltham, MA, USA) equipped with a DC500 digital camera (Leica, Deerfield, IL, USA). FIJI was used to measure average pixel intensity for three images from NTM and GTM cell strains ($n = 3$ each). Data were averaged, and significance was calculated using a 1-way ANOVA.

Immunostaining and Measurement of Cell Size and Cellular Protrusions

For immunostaining experiments, NTM and GTM cell strains (2×10^5 cells/mL) were cultured on collagen I-coated BioFlex plates (FlexCell International Corp, Burlington, NC, USA) for 16 hours. This allowed the cells to adhere, but the cells were not too confluent. Cells were fixed in 4% paraformaldehyde and incubated with CD44 primary antibody (rat monoclonal anti-CD44, clone IM-7; Stem Cell Technologies, Vancouver, BC, Canada) and Alexa-fluor 594-conjugated donkey anti-rat secondary antibody (ThermoFisher). Coverslips were mounted in ProlongGold mounting medium containing 4′,6-diamidino-2-phenylindole (DAPI; ThermoFisher) and visualized using a Fluoview FV1000 confocal microscope (Olympus). Z-stacks were placed 0.5 µm above and 0.5 µm below the fluorescent signal to ensure that the entire cell depth was captured.

The area (μm^2) and volume (μm^3) of NTM and GTM cells were calculated from z-stacks using the "surfaces" module Imaris software (Bitplane, Concord, MA, USA). Partial cells in each image were not counted. If the cells were touching, they were manually separated in the software, and if they could not be easily separated, then those images were discarded. To measure the number and length of filopodia, the "filaments" module was utilized. The start of a protrusion at the cell surface and end of the filaments were manually assigned in the software. To measure the colocalization of Myo10 and cortactin, the "coloc" module was used to produce a Pearson's value, which quantitatively measures the degree of overlap of fluorescent signals acquired in different fluorescent channels.[39] Colocalization was categorized as very strong (0.88–1.0), strong (0.61–0.87), moderate (0.4–0.6), weak (0.13–0.39), and very weak (0–0.12).[40] Actin stress fiber diameters were measured from confocal images by using ImageJ.

Vesicle Transfer Assay

The number of vesicles transferred was quantitated using a vesicle transfer assay.[20,41] Briefly, one flask of confluent TM cells was trypsinized, and half was labeled with Vybrant DiO dye (488 nm), while the other half was labeled with DiD dye (647 nm; ThermoFisher). After washing, fluorescently labeled cells were mixed 1:1, plated at 1×10^5 cells/mL, and incubated overnight. For NTM/GTM coculture assays, NTM ($n = 5$) cells were labeled with DiO and incubated with DiD-labeled GTM ($n = 6$) cells. Cells were then fixed and immunostained with CD44 monoclonal antibody and imaged by confocal microscopy. The total number of DiO (green) and DiD (red) cells were counted in each image. In addition, the number of TM cells containing at least five vesicles of the opposite color "transferred vesicles" was counted. For GTM/NTM cocultures, the percentage of green NTM cells containing red GTM-derived vesicles was calculated, and vice versa.

Live-Cell Imaging of GTM Cells in Culture

GTM or NTM (1×10^5 cells/mL) cells were grown overnight on 4-well micrometer slides (Ibidi USA, Inc., Fitchburg, WI, USA). The following day, 0.1 µM SiR-actin and 10 µM verapamil (Spirochrome, Cytoskeleton, Inc., Denver, CO, USA) were added to the media for 1 hour.[42] Cells were washed with phosphate-buffered saline, and then serum-free Dulbecco's modified Eagle's medium was added. Cells were imaged using a TiE inverted microscope (Nikon, Melville, NY, USA) with a CSU-W1 spinning disk confocal attachment (Yokogawa, Sugar Land, TX, USA). The slides were housed in an enclosed environment that was controlled for humidity and CO_2. Images were acquired on the 647-nm channel by using NIS software (Nikon)

Investigative Ophthalmology & Visual Science

every 2 minutes for 2 hours. Time-lapse movies were made at three frames per second and exported as MP4 files. Individual frames were exported as tifs.

Immunostaining of Human TM Cells and Tissue

NTM and GTM cells were grown in culture overnight, and the next day, the actin cytoskeleton was stained with SiR-actin as above. Cells were fixed and immunostained using rabbit polyclonal Myo10 (PA5-55019; ThermoFisher) and 488-conjugated goat anti-rabbit secondary antibodies. To visualize F-actin and Myo10 in TM tissue, human cadaver eyes were bisected, and the anterior segments, devoid of iris, lens, and ciliary processes, were immersion-fixed in 4% paraformaldehyde. Frontal sections were cut perpendicular to the ocular surface.[43] After permeabilization with 0.02% Tween-20, tissue pieces were incubated overnight with Myo10 primary antibodies, followed by 594-conjugated goat anti-rabbit secondary antibodies. Tissues were immersed in ProLong gold mounting medium containing DAPI and imaged using the Fluoview confocal microscope. Acquisition settings were identical for glaucoma and age-matched NTM tissue. Confocal images were processed postacquisition by using FIJI software.

Statistical Analyses

The number of biologic and technical replicates is noted in each figure legend. Data from GTM and NTM cell strains were averaged, and a standard error of the mean was calculated. $P < 0.05$ by 1-way ANOVA was considered to be statistically significant.

Results

GTM Cell Characterization

Because this study investigates primary GTM cell strains, which can be easily contaminated by other faster growing ocular cell types, several assays were used to characterize the GTM cells. All six GTM cell strains clearly demonstrated increased myocilin protein levels in the media by Western immunoblot following dexamethasone treatment (Fig. 1A). Also, myocilin immunostaining was increased after 7 days of dexamethasone treatment (Figs. 1B, 1C). Cross-linked actin networks are a common feature of GTM cells,[37] which are defined as having "a minimum of three hubs creating at least one triangulated actin arrangement."[44] Characteristic geodesic dome-like cross-linked actin network assemblies were clearly visible in some of our GTM cells (Figs. 1D, 1E). Previous reports indicate that GTM cells had reduced phagocytosis compared to NTM cells.[45] Likewise, our results show a significant reduction in phagocytosis of opsonized pHrodo *S. aureus* bioparticles in GTM cell strains compared to NTM cells (Fig. 1F). Cell size was also measured. CD44 was used to immunostain the TM cell surface, confocal images were acquired (Fig. 1G), and the surfaces module of Imaris software measured the area and volume of the cells (Fig. 1H). GTM cells were 14.8% larger in area (mean, 10; standard error of mean, 467 ± 407 μm^2; $n = 152$ cells) than NTM cells (8913 ± 386 μm^2; $n = 111$ cells) (Fig. 1I). Similarly, GTM cells had a 23% increased volume (20,322 ± 993 μm^3) compared with NTM cells (15,609 ± 960 μm^3) (Fig. 1J). Because cellular senescence can influence cell size and it is a common feature of glaucomatous and aging cells,[46] we measured senescence in our NTM and GTM cell cultures by using senescence-associated β-galactosidase staining. As shown in Figure 1K, there was no significant difference in cellular senescence between NTM and GTM cells. Together, these data confirm that cultured GTM cells have different physical and functional characteristics than NTM cells.

Vesicle Transfer via TNTs in NTM and GTM Cells

Representative images of NTM cells (Figs. 2A–C) and GTM cells (Figs. 2D–F) labeled with the fluorescent Vybrant dyes DiO (green) and DiD (red) are shown. Asterisks denote cells containing vesicles of the opposite color, which were defined as "transferred vesicles." In NTM cells ($n = 406$), approximately 35% of cells contained transferred vesicles after 16 hours of incubation (Fig. 2G), which is similar to our previously reported percentage.[20] In GTM cells ($n = 466$), there was a significant increase in the percentage of cells containing transferred fluorescent vesicles (49.6%; $P = 0.0001$). Coculture experiments in other cell types suggest the formation of heterotypic TNTs between two different cell types.[47–49] Therefore, we cocultured GTM (red) and NTM (green) cells for 16 hours and measured vesicle transfer (Figs. 3A–H). Arrows point to cells that were either NTM or GTM cells, while asterisks denote cells containing transferred vesicles of the opposite color. A long TNT, approximately 140 μm in length and 2.1 μm in diameter, extended between a GTM cell (red) and NTM cell (green) (Fig. 3D). At higher magnification, DiD- and DiO-labeled vesicles were clearly shown within the long protrusion (Figs. 3E–H). Cell counts of NTM ($n = 418$) and GTM ($n = 370$) showed that there were significantly more red GTM vesicles transferred to NTM cells (57.8%) than green NTM vesicles transferred to GTM cells (43.3%; $P = 0.0001$) (Fig. 3I).

Number and Length of TM Cellular Protrusions

Because there appears to be a relationship between the length of cellular protrusions and TNT formation, the number and length of cellular protrusions emanating from the TM cell surface was measured using the filaments module of Imaris software (Figs. 4A, 4B). Because there are no biomarkers that distinguish filopodia from TNTs, all cellular protrusions were measured. The average number of protrusions per cell was significantly increased for NTM cells (7.61 ± 0.71; $n = 60$ cells) compared to GTM cells (4.65 ± 0.58; $n = 68$ cells) (Fig. 4C). Conversely, the average length of the filaments was increased in GTM cells (12.1 μm ± 0.55; $n = 306$ filaments) compared to NTM cells (9.76 μm ± 0.34; $n = 459$ filaments) (Fig. 4D). Distribution analysis demonstrated that NTM cells had a higher number of short filopodia than GTM cells (Fig. 4E). When represented as a percentage of the total number, 65% NTM cellular protrusions were 0 to 10 μm long, whereas 42% of GTM cells had >10-μm protrusions (Fig. 4F). Collectively, our data show that GTM cells had 40% fewer cellular protrusions, but they were approximately 19% longer than NTM cells.

Actin Dynamics in Live Cells

Actin is a core component of TNTs.[16] Therefore, we used SiR-actin to stain NTM and GTM cells and visualized the actin cytoskeleton by live-cell imaging. In NTM cells, actin stress fibers were of variable diameter and displayed a predominantly parallel arrangement (Fig. 5A; Supplementary Video S1). All but the thickest actin stress fibers were turned over during the 2-hour acquisition time. Highly dynamic punctate SiR-actin-labeled vesicles were also evident, some of which were transferred between cells (Fig. 5B). Each panel shows a frame from the movie at 2-minute intervals. Within 32 minutes, three vesicles were transferred from one cell to another. In each case, the vesicle moved to the tip of an actin protrusion of the donor cell (t = 96 minutes), and then the vesicle became

Investigative Ophthalmology & Visual Science

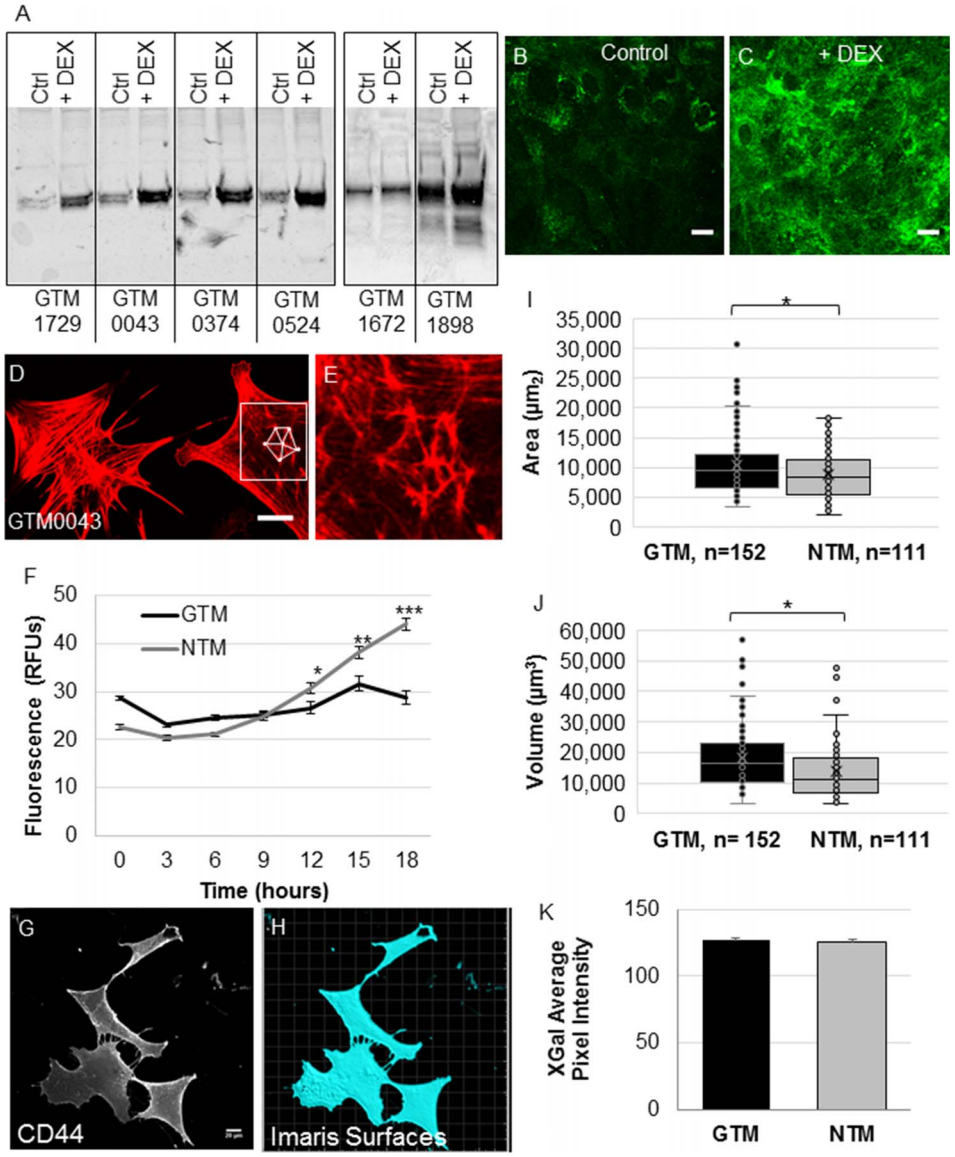

Figure 1. Characterization of primary GTM cell cultures. (**A**) Western immunoblots of myocilin induction by dexamethasone treatment of GTM cells. (**B**, **C**) Myocilin immunostaining of GTM cells with and without dexamethasone treatment for 7 days. *Scale bar*: 20 μm. (**D**, **E**) SiR-actin stained GTM cells (*red*) with a cross-linked actin network (CLAN) formation overlayed (*white*). Boxed area is shown at higher magnification to show the characteristic geodesic CLAN formation. *Scale bar*: 20 μm. (**F**) Phagocytosis assay of GTM versus NTM cells. Three technical replicates using GTM ($n = 3$) and NTM ($n = 3$) cells were performed. $^{*}P < 0.05$; $^{**}P < 0.005$; $^{***}P < 0.0005$. (**G**) Representative CD44-immunostained image of a NTM cell. (**H**) Imaris surfaces image showing the filled-in portion (cyan) of four cells that were measured. (**I**) Imaris software measured the area of GTM ($n = 152$) and NTM ($n = 111$) cells. $^{*}P = 0.011$ by ANOVA. (**J**) Imaris software measured the volume in GTM ($n = 152$) and NTM ($n = 111$) cells. $^{*}P = 0.0001$ by ANOVA. For area and volume measurements, GTM ($n = 5$ biologic replicates) and NTM ($n = 5$ biologic replicates). The "X" is the mean and the line is the median. (**K**) Average pixel intensity of senescence-associated β-galactosidase-stained NTM and GTM cells ($n = 3$ each).

associated with the tip of a short actin assembly in the recipient cell as if it were being pushed across by the actin (t = 98–100 minutes). After the transfer was complete, the actin protrusion on the donor cell disassembled. This process was repeated in turn for the remaining two vesicles. The transfer of vesicles via the TNT coincided with the localized disassembly of the actin cortex on the same side of the cell as the TNT was formed (arrows). However, cortical actin underlying the TNT and on the other two sides of the cell (arrowheads) was unaffected. Thus, it remains unclear if the actin involved in vesicle transfer was derived from actin stress fibers or cortical actin.

The actin cytoskeleton of GTM cells was different (Fig. 6A; Supplementary Video S2). Actin stress fibers of GTM cells appeared thicker than in NTM cells, and there was little disassembly of stress fibers, most of which were unaltered during the 120-minute acquisition time. Actin-rich cellular protrusions were noticeable emanating from the cell surface, but they were more stable than NTM cells. Punctate SiR-actin-labeled vesicles were present, but they moved at a slower rate than vesicles in NTM cells. In the video, one actin-rich vesicle was shown to transfer between cells (Fig. 6B), but the transfer mechanism appeared different than in NTM cells. A thin actin-rich protrusion emanated from each of the adjacent cells (t = 12 minutes). The protrusions then appeared to touch (t = 30 minutes) and fuse (t = 66 minutes). Contrary to NTM cells, the vesicle was not at the tip of the donor cell protrusion, but rather the vesicle only seemed to travel once a TNT became

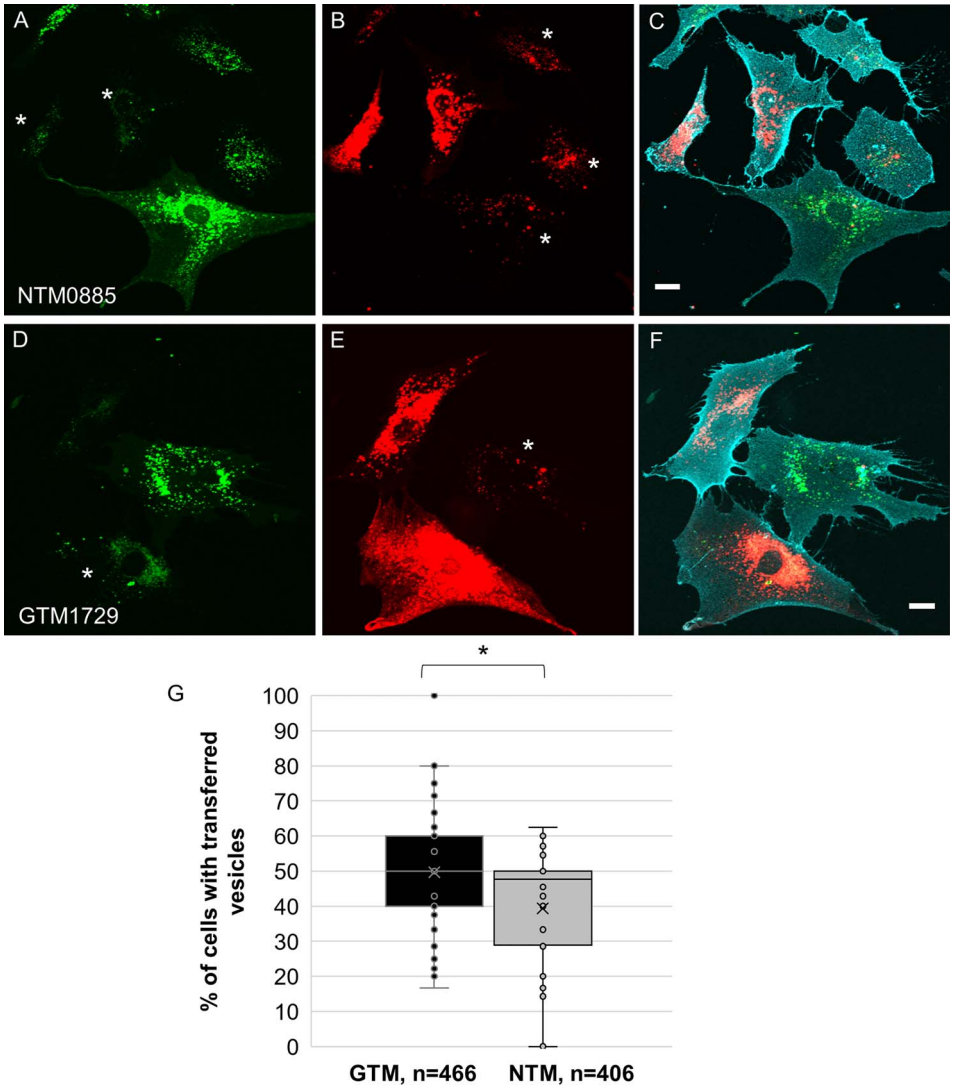

Figure 2. Vesicle transfer in GTM and NTM cell strains. (**A**–**C**) NTM cells were labeled with either (**A**) DiO (*green*) or (**B**) DiD (*red*), mixed 1:1, and then grown for 16 hours. The cell strain is noted. (**C**) Merged image showing the CD44-immunostained cell membrane. Asterisks indicate cells containing >5 vesicles of the opposite color, which were designated as containing transferred vesicles. *Scale bar*: 20 µm. (**D**–**F**) A similar experiment using a GTM cell strain (2017-1729). (**G**) The number of cells with transferred vesicles was counted in GTM ($n = 466$) or NTM ($n = 406$) cell strains. Data from eight NTM and six GTM cell strains were combined. The "X" is the mean and the line is the median. *$P = 0.0001$ by ANOVA.

established. This entire process also took a lot longer (>100 minutes) than in NTM cells and transfer to the recipient cell may not have been fully complete. However, similar to NTM cells, cortical actin on the same side of the cell as the TNT connection appeared to be partially disassembled during vesicle transfer, whereas the actin cortex on the other sides remained intact. In addition to vesicle transfer via TNTs, an actin ring-like structure was observed (Fig. 6C). This was comparable in size (0.5–1 µm) to that described for podosomes and invadopodia-like structures (PILSs).[18,50] Over the course of 108 mins, the actin at the outer edges of the ring thickened. The actin core was sometimes visible as a dot in the center of the ring.

Myosin-10 Distribution in GTM Cells and Tissue

Because Myo10 is involved in TNT and filopodia formation,[12,13] we investigated the distribution of Myo10 in normal and GTM cells (Fig. 7) and tissue (Fig. 8). By immunofluorescence, Myo10 (green) was distributed in PILS-like structures in NTM cells (Figs. 7A–H). SiR-stained actin (red) is also shown (Figs. 7B, 7F, 7J, 7N). In GTM cells (Figs. 7I–P), Myo10 was found in PILSs, but the ring-like structures were not as clearly defined and had a smaller diameter than PILSs in NTM cells. Similar to live cells, increased actin stress fibers with thick diameters were readily apparent in GTM cells. Punctate Myo10 was visible, but the immunostaining was not associated with filopodia tips. Higher magnification images of Myo10 in the rosettes are also shown where the immunostaining colocalized with actin (Figs. 7D, 7L) or cortactin (Figs. 7H, 7P). By immunofluorescence, Myo10 levels appeared to be increased in GTM cells, so Western immunoblots were performed to quantitate Myo10 protein levels in GTM ($n = 6$) and NTM ($n = 9$) cell strains (Fig. 7Q). Densitometry showed no significant differences in Myo10 protein levels. Colocalization of Myo10 and cortactin was quantitated using the coloc module of Imaris software (Fig. 7S). In NTM cells, Myo10 and cortactin were strongly colocalized, with an average Pearson's value of 0.724 ± 0.014. Yet, GTM cells had a significantly lower average Pearson's value of 0.5988 ± 0.016, which is designated as

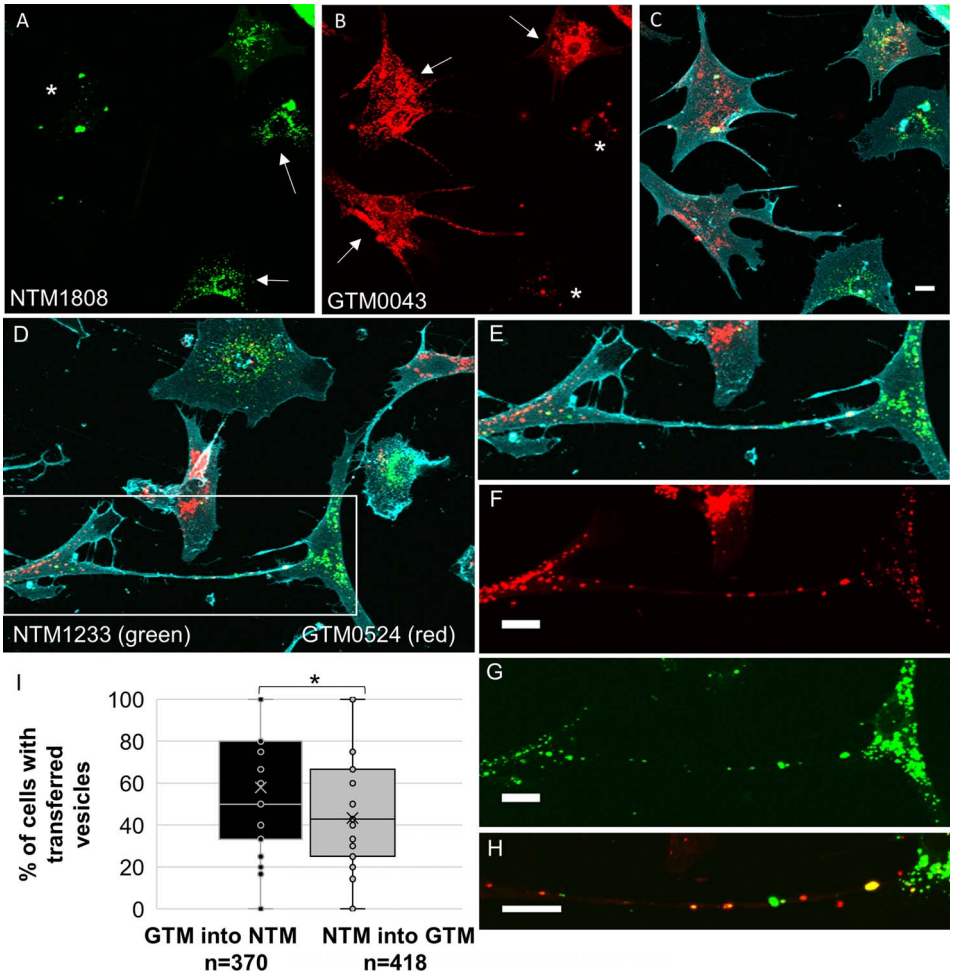

Figure 3. Vesicle transfer in cocultures of NTM and GTM cells. (**A**–**C**) DiO-labeled NTM cells (2011-1808; *green*) were cocultured with DiD-labeled GTM cells (2018-0043; *red*) for 16 hours. *White arrows* show cells that were considered either (**A**) NTM or (**B**) GTM, while *asterisks* show cells containing >5 transferred vesicles of the opposite color. (**C**) Merged image showing the CD44-immunostained cell membrane. *Scale bar*: 20 µm. (**D**) Confocal image of a long TNT connecting a GTM cell (2018-0524; *red*) to a NTM cell (2018-1233; *green*). Boxed area is shown at higher magnification in panels (**E**–**H**). *Red* and *green vesicles* are clearly seen within the TNT. (**I**) The percentage of GTM cells containing NTM vesicles ($n = 370$) or NTM cells containing GTM vesicles ($n = 418$) were measured. Data were combined from NTM ($n = 8$) and GTM ($n = 6$) cell strains. The "X" is the mean and the line is the median. $^*P = 0.0001$ by ANOVA.

"moderate" colocalization.[40] Moreover, GTM cells had significantly thicker stress fibers than NTM cells (Fig. 7T).

Myo10 protein distribution in glaucomatous ($n = 3$; average age, 85.3 ± 4.5 years; range, 81–90 years) and age-matched normal human TM tissue ($n = 4$; 82.2 ± 7.7 years; range, 73–90 years) was investigated. In en face images of NTM tissue, the Myo10 protein appears perinuclearly and in long cellular processes (Figs. 8B, 8G). However, in GTM tissue, Myo10 immunostaining (red) was primarily punctate, with some cells showing perinuclear staining (Figs. 8E, 8H). Together, our data show that there was a disruption of Myo10 protein localization in GTM tissue compared to age-matched NTM.

Discussion

A direct method of cellular communication via TNTs is advantageous for cells in the anterior of the eye, which are bathed in aqueous humor fluid. Aqueous environments hinder communication via more traditional diffusion-based mechanisms because signaling molecules are diluted and washed away before binding to their target receptors. Therefore, diffusion-based signaling is limited to cells in close proximity to the secretory cell. Because cellular communication is inherent to the normal homeostatic function of any tissue, the discovery of TNTs in NTM cells represents a major advance in the field of TM cell biology.[20] However, the emerging role of TNTs in pathologic disease, including neurodegenerative diseases such as glaucoma, remains poorly understood.[24,25] In this study, we showed that the cellular protrusions emanating from GTM cells have different phenotypic and functional characteristics than NTM cells.

GTM cells had fewer filopodia at the cell surface than NTM cells. This lower number could negatively impact TNT formation because TNTs can form by fusing the membrane tips of filopodia from adjacent cells.[4] However, it is possible that filopodia on GTM cells are reduced because they form more TNT connections, which has been described for neuronal cells.[12] Thus, there may be a regulated balance between filopodia and TNTs. Certainly, our GTM cells had increased vesicle transfer compared to NTM cells, which is suggestive of more TNT connections. Further studies are required to investigate whether increased vesicle transfer is due to a switch from filopodia to TNT formation in GTM cells.

Recent studies have described a multicycle role of Myo10 in filopodia elongation.[14,51] In the first step, Myo10 initiated

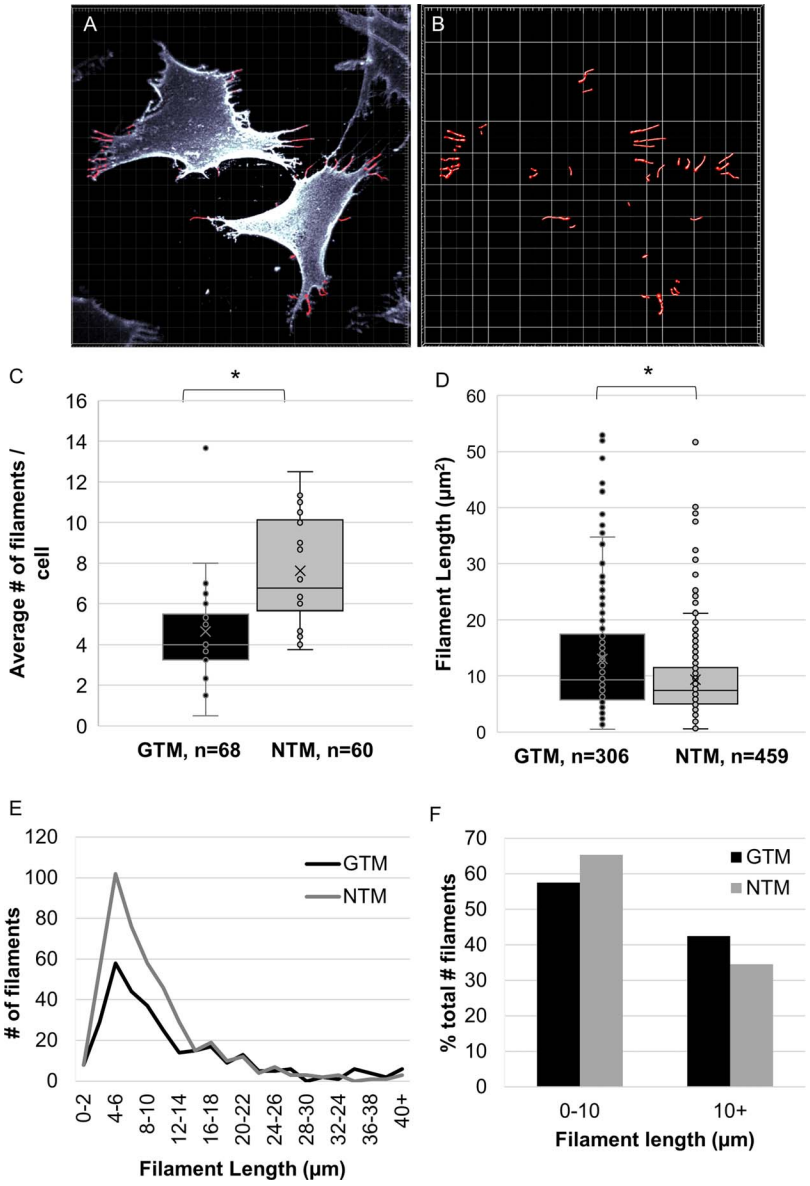

Figure 4. The number and length of cellular protrusions. (**A**) Representative CD44-immunostained image of a NTM cell. The "filaments" module of Imaris software assigned the beginning and end point of each cellular protrusion (*red*). (**B**) Imaris image showing the filaments without the CD44 channel. (**C**) The number of cellular protrusions emanating from the cell surface of GTM ($n = 68$) and NTM ($n = 60$) cells was counted using Imaris software. $^*P = 0.0001$. (**D**) The length of the filaments in GTM ($n = 306$) and NTM ($n = 459$) cells. $^*P = 0.0001$. (**E**) Distribution of filament length in GTM and NTM cells grouped into lengths of 2 µm. (**F**) Bar chart showing the percentage of filaments that were either 0 to 10 µm or >10 µm long for NTM and GTM cells.

filopodia formation at the cell membrane, giving rise to short protrusions approximately 2 µm long. Myo10 then relocated to the tip of the filopodia and formed a transient attachment to the underlying substrate. While the tip was attached, additional Myo10 and Arp2/3 were recruited and a second step of elongation occurred, lengthening the filopodia to approximately 4 µm.[14,51] In this study, we showed that GTM cells had more stable actin and Myo10 distribution was more punctate. Stabilized actin may provide a platform to promote a more efficient recruitment of Myo10 and Arp2/3 to extend filopodia. Hence, the observed increase in filopodia length.

Live-cell imaging showed that actin dynamics are impaired in GTM cells. Over a 2-hour period, there was little disassembly of stress fibers, and actin-rich punctate vesicles moved more slowly than in NTM cells. One vesicle took >100 minutes to transfer in GTM cells compared to three vesicles transferred in 32 minutes in NTM cells. This slower rate of transfer could severely impact the rapid communication of signals required during pressure increases in the eye in vivo. Yet, surprisingly, our vesicle transfer assay indicated that GTM cells contained significantly more transferred vesicles than NTM cells. We speculate that altered actin dynamics led to more prolonged TNT connections in GTM cells, thus allowing more vesicles to transfer between cells over the 16-hour duration of the experiment. Our data also suggest that different mechanisms may contribute to vesicle transfer in NTM and GTM cells. In NTM cells, an actin-driven mechanism propelled the transfer of vesicles via TNTs, whereas a TNT was formed before vesicle transfer occurred in GTM cells. Our data suggest that different TNT mechanisms affect transfer rate. This could have major effects in vivo because the rapid transmission of cellular signals related to IOP changes may be hindered in GTM cells.

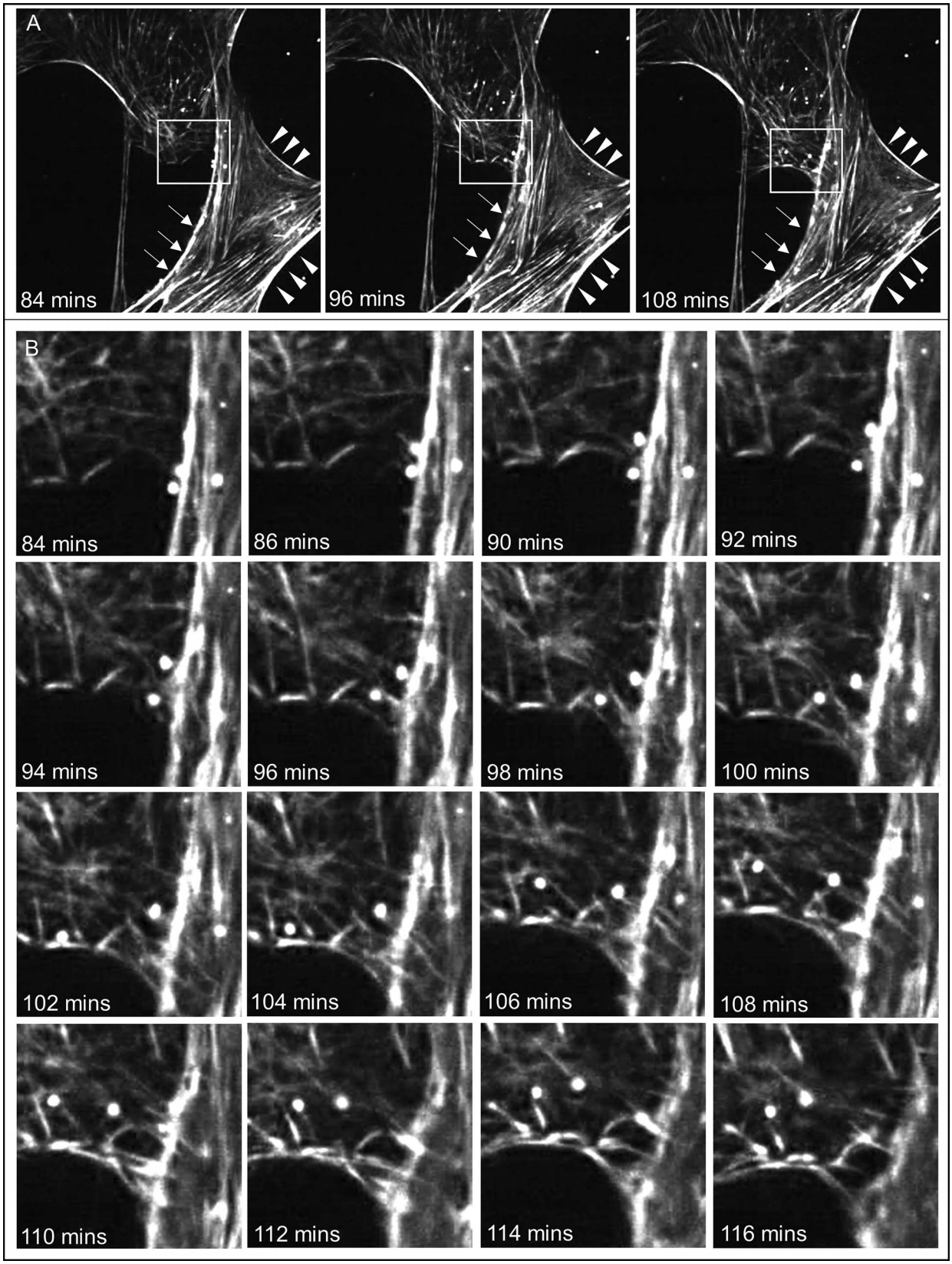

Figure 5. Images from live-cell imaging of the actin cytoskeleton of NTM cells. (**A**) Three panels show NTM cells stained with SiR-actin at 84, 96, and 108 minutes. *Arrows* point to cortical actin on the same side as the emerging TNT, while *arrowheads* denote cortical actin on the other two sides of the cell. The *boxed area* is shown at higher magnification in (**B**). Sixteen panels show the transfer of three vesicles from a donor cell on the right to a recipient cell on the left at 2-minute intervals.

Investigative Ophthalmology & Visual Science

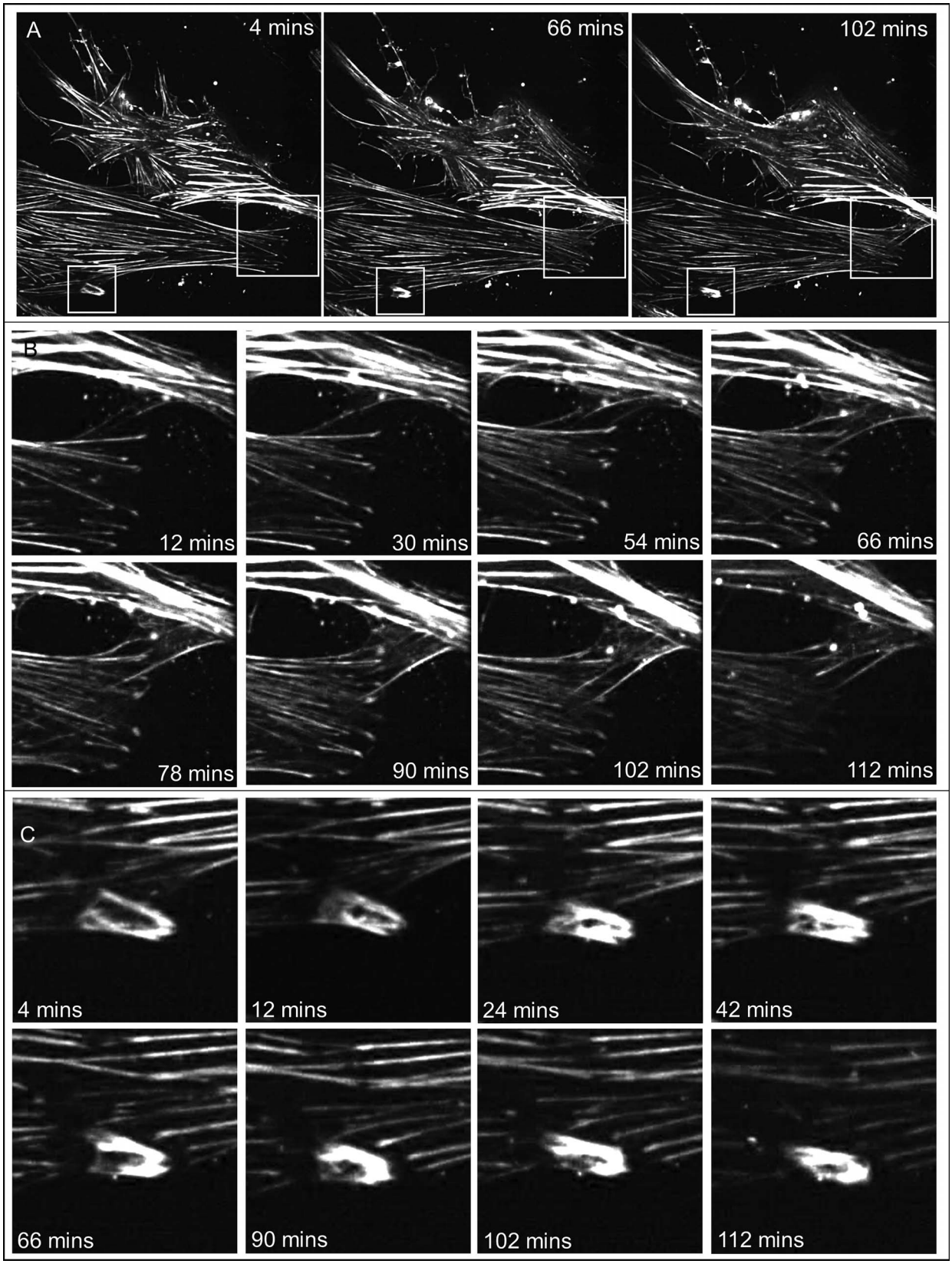

Figure 6. Images from live-cell imaging of the actin cytoskeleton of GTM cells. (**A**) Three panels show GTM cells stained with SiR-actin at 4, 66, and 102 minutes. The *larger boxed area* is shown at higher magnification in (**B**), while the *smaller box* is shown in (**C**). (**B**) Eight panels show the transfer of one vesicles from a donor cell at the top to a recipient cell at the bottom over 100 minutes. (**C**) Eight panels show the formation of a podosome actin ring-like structure from 4 to 112 minutes. An actin core is visible at 12, 42, and 102 minutes.

Investigative Ophthalmology & Visual Science

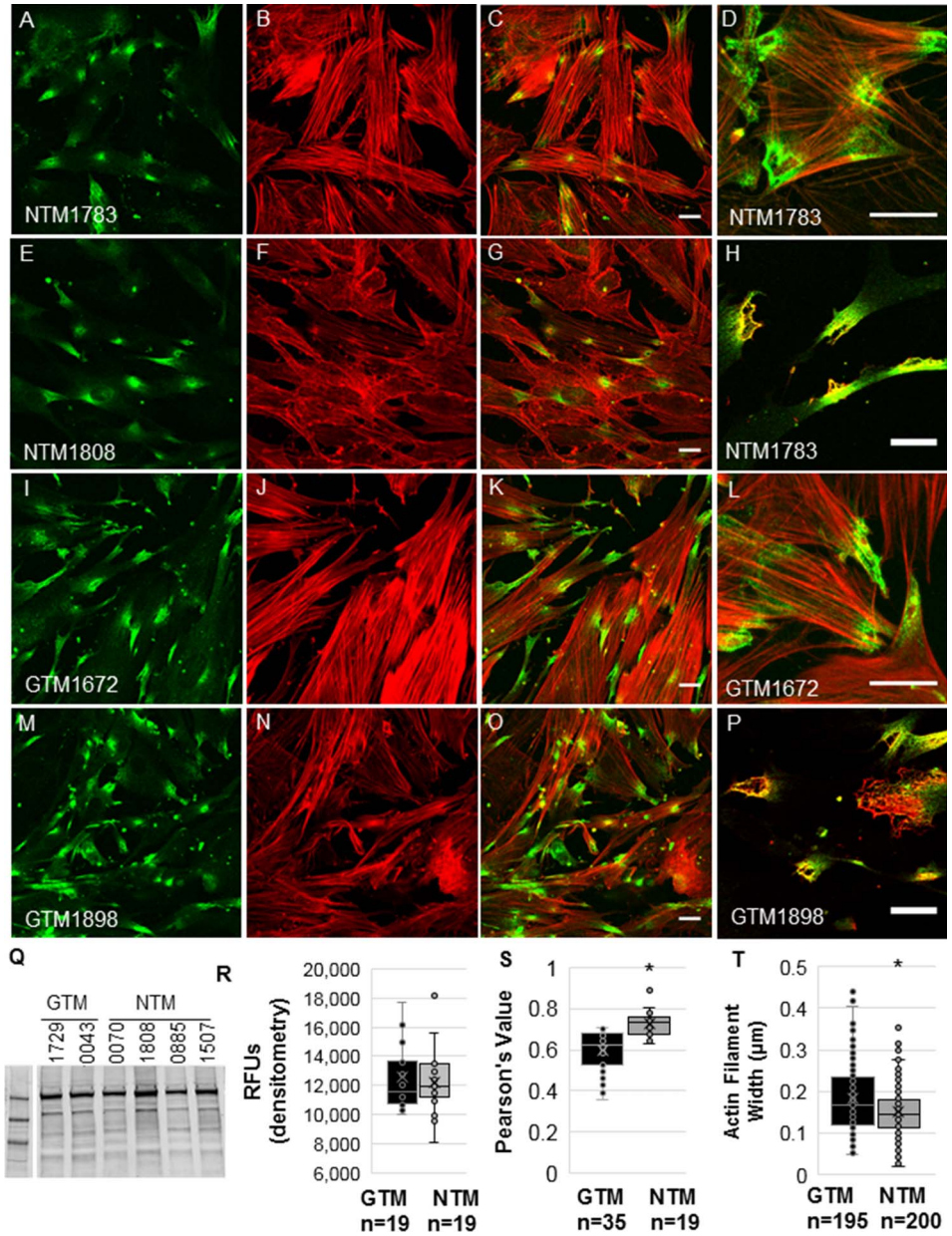

Figure 7. Myo10 protein distribution in NTM and GTM cells. Myo10 (*green*) and SiR-actin (*red*) in two NTM cell strains (**A–G**) and two GTM cell strains (**I–O**). Myo10 colocalized with cortactin in NTM cells (**H**) and GTM cells (**P**). *Scale bars*: 20 μm. (**Q**) Western immunoblotting showing Myo10 protein levels in GTM ($n = 2$) and NTM cells ($n = 4$). (**R**) Densitometry of Western immunoblots ($n = 19$ technical replicates) of GTM ($n = 6$ biologic replicates) and NTM ($n = 9$ biologic replicates). (**S**) Pearson's colocalization values of Myo10 and cortactin in GTM ($n = 35$) and NTM ($n = 19$) cells. (**T**) The diameter of actin stress fibers was calculated in GTM ($n = 195$) and NTM ($n = 200$) cells. *$P = 0.0001$.

In both NTM and GTM cells, cortical actin appeared to play a role in TNT formation. Although cortical actin underlying the emerging TNT was not dramatically affected, there was a large decrease in cortical actin in regions on the same side of the cell concomitant with emergence of a TNT. Cortical actin is a network of thin actin filaments that form a dense meshwork underlying the plasma membrane.[52] Interestingly, cortical actin is prevalent in TM tissue in situ, whereas stress fibers are not.[53] The density of the actin cortex is dependent on the levels of mDia1, a formin, and Arp2.[54] When mDia was inhibited, the actin cortex density was decreased, whereas inhibiting Arp2 increased cortical actin filament length. Eps8, the actin filament bundler that drives TNT formation,[55] also bundles cortical actin filaments.[52] Thus, the same actin-binding proteins appear to regulate TNT formation and cortical actin. Further studies are required to delineate the potential relationship between the actin cortex and TNTs.

Previously, we showed increased vesicle transfer in TM cells treated with the ROCK inhibitor Y27632, which disassembles stress fibers.[20] Thus, disassembly of actin stress fibers and more stable actin in GTM cells both lead to increased vesicle transfer. It is possible that actin-binding TNT regulators are differentially expressed in GTM cells compared to Y27632-treated NTM cells. In other cell types, the altered expression of actin-binding proteins leads to changes in TNTs. For instance, ectopic expression of M-sec, Eps8, or LST1 not only increases the number of filopodia but also increases TNT connections.[10,12,55,56] Alternatively, microtubules may be involved

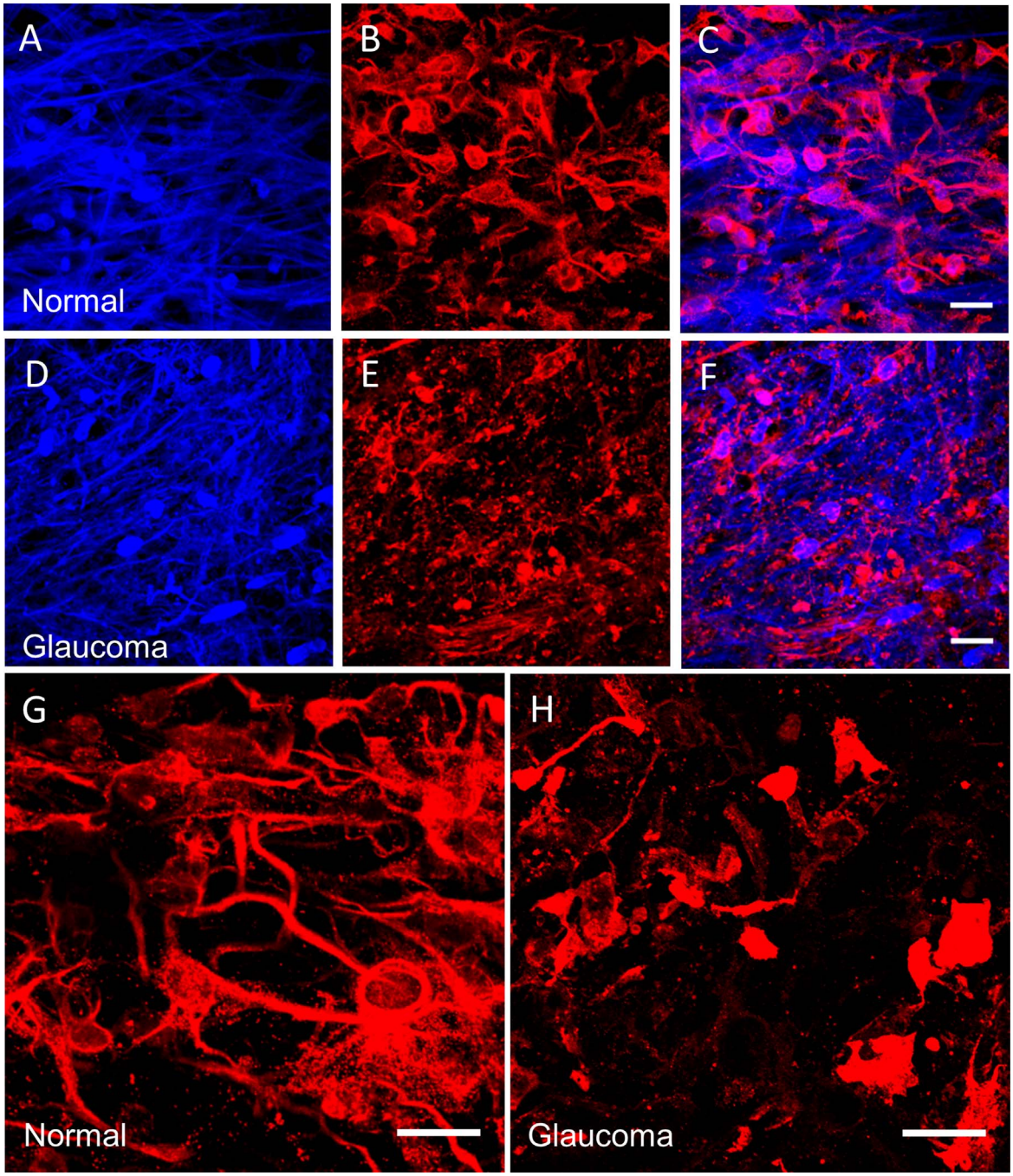

Figure 8. Myo10 protein distribution in age-matched normal and glaucomatous human TM tissue. Myo10 protein (*red*) distribution in en face images of normal (**A–C**, **G**) and glaucomatous (**D–F**, **H**) TM tissue. *Blue* is DAPI-stained nuclei and autofluorescence of TM tissue. *Scale bars*: 20 μm.

because microtubules are associated with TNTs that are >0.7 μm in diameter, such as in GTM cells.[57] It is also possible that the vesicle transfer assay measures changes via exosome release/uptake in addition to direct transfer via TNTs. Potential changes in exosome transfer between GTM and NTM cells, or between Y27632-treated NTM cells, have not yet been examined. Podosomes are cellular structures composed of an actin ring and core that are involved in adhesion and matrix degradation.[58] They are dynamic structures with a reported half-life of 2 to 12 minutes. Here, the ring-like structure in GTM cells was apparent for the entire 120-minute duration of the experiment, which again indicates that actin is stabilized and not dynamic in GTM cells. Myo10 distribution was also disrupted in GTM cells and Myo10-stained PILSs had a smaller diameter than NTM cells. Our results are consistence with a prior study that shows that small interfering RNA knock down of Myo10 resulted in smaller podosome sealing rings in osteoclasts.[17] Furthermore, changes in PILSs may impact extracellular matrix degradation because Myo10 knock down led to reduced matrix metalloproteinase activity.[18]

There are several limitations in this study. The glaucoma cadaver eyes usually come with an incomplete history so that we often do not know the IOP history or the glaucoma medications they were prescribed. However, all six of the GTM cell strains used in this study showed similar differences in actin dynamics and Myo10 distribution described. GTM cells

were derived from older individuals than NTM cells, so actin dynamics may be influenced by age of the donor. Another caveat is that our cellular protrusion measurements were based on CD44 immunostaining of the cell membrane, and it is possible that CD44 redistribution in GTM and NTM cells influenced our measurements. However, measurement of SiR-actin-labeled protrusions showed a similar trend (data not shown). There remains a possibility that SiR-actin, a jasplakinolide analog, stabilizes actin filaments. Although prior studies showed that 100 nM jasplakinolide affected actin dynamics, 100 nM SiR-actin did not.[42] In this study, we used 100 nM SiR-actin to treat GTM and NTM cells, and our live-cell imaging data show that in NTM cells, actin filaments are disassembled over the 2-hour time frame. Furthermore, SiR-stained actin stress fibers were rapidly disassembled by treatment with Y27632, a Rho kinase inhibitor.[20] This argues that even if SiR-actin affects actin assembly, the effects are reversible and are not long term.

In summary, we have shown that GTM cells have phenotypic and functional changes to their TNTs due to a more stable actin cytoskeleton and Myo10 redistribution. Our study also suggests that the actin cortex may be involved in TNT formation. Significantly slower vesicle transfer via TNTs in GTM cells may delay the timely propagation of cellular signals when pressures become elevated in glaucoma. Future studies aim to elucidate the molecular pathways involved in TNT function in normal and GTM cells to further investigate the role of TNTs in outflow regulation and IOP homeostasis.

Acknowledgments

The authors thank Lions VisionGift, Portland, Oregon for facilitating the procurement of human donor eyes and the Advanced Light Microscopy core facility at Oregon Health & Sciences University, Portland, Oregon for help with the live-cell imaging.

Supported by National Institute of Health RO1 grants EY019643 and EY010572 (P30 Casey Eye Institute Core facility grant) and an unrestricted grant to the Casey Eye Institute from Research to Prevent Blindness, New York, New York, United States.

Disclosure: **Y.Y. Sun**, None; **J.M. Bradley**, None; **K.E. Keller**, None

References

1. Gerdes HH, Rustom A, Wang X. Tunneling nanotubes, an emerging intercellular communication route in development. *Mech Dev*. 2013;130:381–387.
2. Marzo L, Gousset K, Zurzolo C. Multifaceted roles of tunneling nanotubes in intercellular communication. *Front Physiol*. 2012;3:72.
3. Davis DM, Sowinski S. Membrane nanotubes: dynamic long-distance connections between animal cells. *Nat Rev Mol Cell Biol*. 2008;9:431–436.
4. Rustom A, Saffrich R, Markovic I, Walther P, Gerdes HH. Nanotubular highways for intercellular organelle transport. *Science*. 2004;303:1007–1010.
5. Dupont M, Souriant S, Lugo-Villarino G, Maridonneau-Parini I, Verollet C. Tunneling nanotubes: intimate communication between myeloid cells. *Front Immunol*. 2018;9:43.
6. Gurke S, Barroso JF, Hodneland E, Bukoreshtliev NV, Schlicker O, Gerdes HH. Tunneling nanotube (TNT)-like structures facilitate a constitutive, actomyosin-dependent exchange of endocytic organelles between normal rat kidney cells. *Exp Cell Res*. 2008;314:3669–3683.
7. Osteikoetxea-Molnar A, Szabo-Meleg E, Toth EA, et al. The growth determinants and transport properties of tunneling nanotube networks between B lymphocytes. *Cell Mol Life Sci*. 2016;73:4531–4545.
8. Takahashi A, Kukita A, Li YJ, et al. Tunneling nanotube formation is essential for the regulation of osteoclastogenesis. *J Cell Biochem*. 2013;114:1238–1247.
9. Wang Y, Cui J, Sun X, Zhang Y. Tunneling-nanotube development in astrocytes depends on p53 activation. *Cell Death Differ*. 2011;18:732–742.
10. Hase K, Kimura S, Takatsu H, et al. M-Sec promotes membrane nanotube formation by interacting with Ral and the exocyst complex. *Nat Cell Biol*. 2009;11:1427–1432.
11. Berg JS, Cheney RE. Myosin-X is an unconventional myosin that undergoes intrafilopodial motility. *Nat Cell Biol*. 2002;4:246–250.
12. Gousset K, Marzo L, Commere PH, Zurzolo C. Myo10 is a key regulator of TNT formation in neuronal cells. *J Cell Sci*. 2013;126:4424–4435.
13. Bohil AB, Robertson BW, Cheney RE. Myosin-X is a molecular motor that functions in filopodia formation. *Proc Natl Acad Sci U S A*. 2006;103:12411–12416.
14. Watanabe TM, Tokuo H, Gonda K, Higuchi H, Ikebe M. Myosin-X induces filopodia by multiple elongation mechanism. *J Biol Chem*. 2010;285:19605–19614.
15. Kerber ML, Cheney RE. Myosin-X: a MyTH-FERM myosin at the tips of filopodia. *J Cell Sci*. 2011;124:3733–3741.
16. Berg JS, Derfler BH, Pennisi CM, Corey DP, Cheney RE. Myosin-X, a novel myosin with pleckstrin homology domains, associates with regions of dynamic actin. *J Cell Sci*. 2000;113Pt 19:3439–3451.
17. McMichael BK, Cheney RE, Lee BS. Myosin X regulates sealing zone patterning in osteoclasts through linkage of podosomes and microtubules. *J Biol Chem*. 2010;285:9506–9515.
18. Sun YY, Yang YF, Keller KE. Myosin-X silencing in the trabecular meshwork suggests a role for tunneling nanotubes in outflow regulation. *Invest Ophthalmol Vis Sci*. 2019;60:843–851.
19. Hetrick B, Han MS, Helgeson LA, Nolen BJ. Small molecules CK-666 and CK-869 inhibit actin-related protein 2/3 complex by blocking an activating conformational change. *Chem Biol*. 2013;20:701–712.
20. Keller KE, Bradley JM, Sun YY, Yang YF, Acott TS. Tunneling nanotubes are novel cellular structures that communicate signals between trabecular meshwork cells. *Invest Ophthalmol Vis Sci*. 2017;58:5298–5307.
21. Hanna SJ, McCoy-Simandle K, Miskolci V, et al. The role of Rho-GTPases and actin polymerization during macrophage tunneling nanotube biogenesis. *Sci Rep*. 2017;7:8547.
22. Gousset K, Schiff E, Langevin C, et al. Prions hijack tunnelling nanotubes for intercellular spread. *Nat Cell Biol*. 2009;11:328–336.
23. Sowinski S, Jolly C, Berninghausen O, et al. Membrane nanotubes physically connect T cells over long distances presenting a novel route for HIV-1 transmission. *Nat Cell Biol*. 2008;10:211–219.
24. Mittal R, Karhu E, Wang JS, et al. Cell communication by tunneling nanotubes: implications in disease and therapeutic applications. *J Cell Physiol*. 2019;234:1130–1146.
25. Jash E, Prasad P, Kumar N, Sharma T, Goldman A, Sehrawat S. Perspective on nanochannels as cellular mediators in different disease conditions. *Cell Commun Signal*. 2018;16:76.
26. Cao R, Chen J, Zhang X, et al. Elevated expression of myosin X in tumours contributes to breast cancer aggressiveness and metastasis. *Br J Cancer*. 2014;111:539–550.
27. Quigley HA. Glaucoma. *Lancet*. 2011;377:1367–1377.
28. Acott TS, Kelley MJ, Keller KE, et al. Intraocular pressure homeostasis: maintaining balance in a high-pressure environment. *J Ocul Pharmacol Ther*. 2014;30:94–101.
29. Vranka JA, Kelley MJ, Acott TS, Keller KE. Extracellular matrix in the trabecular meshwork: intraocular pressure regulation

and dysregulation in glaucoma. *Exp Eye Res*. 2015;133:112–125.

30. Kaufman PL, Rasmussen CA. Advances in glaucoma treatment and management: outflow drugs. *Invest Ophthalmol Vis Sci*. 2012;53:2495–2500.
31. Tian B, Gabelt BT, Geiger B, Kaufman PL. The role of the actomyosin system in regulating trabecular fluid outflow. *Exp Eye Res*. 2009;88:713–717.
32. Rao PV, Deng PF, Kumar J, Epstein DL. Modulation of aqueous humor outflow facility by the Rho kinase-specific inhibitor Y-27632. *Invest Ophthalmol Vis Sci*. 2001;42:1029–1037.
33. Inoue T, Tanihara H. Rho-associated kinase inhibitors: a novel glaucoma therapy. *Prog Retin Eye Res*. 2013;37:1–12.
34. Raghunathan VK, Benoit J, Kasetti R, et al. Glaucomatous cell derived matrices differentially modulate non-glaucomatous trabecular meshwork cellular behavior. *Acta Biomater*. 2018; 71:444–459.
35. Porter K, Hirt J, Stamer WD, Liton PB. Autophagic dysregulation in glaucomatous trabecular meshwork cells. *Biochim Biophys Acta*. 2015;1852:379–385.
36. Hoare MJ, Grierson I, Brotchie D, Pollock N, Cracknell K, Clark AF. Cross-linked actin networks (CLANs) in the trabecular meshwork of the normal and glaucomatous human eye in situ. *Invest Ophthalmol Vis Sci*. 2009;50:1255–1263.
37. Clark AF, Miggans ST, Wilson K, Browder S, McCartney MD. Cytoskeletal changes in cultured human glaucoma trabecular meshwork cells. *J Glaucoma*. 1995;4:183–188.
38. Keller KE, Bhattacharya SK, Borras T, et al. Consensus recommendations for trabecular meshwork cell isolation, characterization and culture. *Exp Eye Res*. 2018;171:164–173.
39. Zinchuk V, Zinchuk O, Okada T. Quantitative colocalization analysis of multicolor confocal immunofluorescence microscopy images: pushing pixels to explore biological phenomena. *Acta Histochem Cytochem*. 2007;40:101–111.
40. Zinchuk V, Wu Y, Grossenbacher-Zinchuk O. Bridging the gap between qualitative and quantitative colocalization results in fluorescence microscopy studies. *Sci Rep*. 2013;3:1365.
41. Abounit S, Delage E, Zurzolo C. Identification and characterization of tunneling nanotubes for intercellular trafficking. *Curr Protoc Cell Biol*. 2015;67:12.10.
42. Lukinavicius G, Reymond L, D'Este E, et al. Fluorogenic probes for live-cell imaging of the cytoskeleton. *Nat Methods*. 2014;11:731–733.
43. Lu Z, Overby DR, Scott PA, Freddo TF, Gong H. The mechanism of increasing outflow facility by rho-kinase inhibition with Y-27632 in bovine eyes. *Exp Eye Res*. 2008; 86:271–281.
44. Montecchi-Palmer M, Bermudez JY, Webber HC, Patel GC, Clark AF, Mao W. TGFbeta2 induces the formation of cross-linked actin networks (CLANs) in human trabecular meshwork cells through the Smad and non-Smad dependent pathways. *Invest Ophthalmol Vis Sci*. 2017;58:1288–1295.
45. Zhang X, Ognibene CM, Clark AF, Yorio T. Dexamethasone inhibition of trabecular meshwork cell phagocytosis and its modulation by glucocorticoid receptor beta. *Exp Eye Res*. 2007;84:275–284.
46. Liton PB, Challa P, Stinnett S, Luna C, Epstein DL, Gonzalez P. Cellular senescence in the glaucomatous outflow pathway. *Exp Gerontol*. 2005;40:745–748.
47. Islam MN, Das SR, Emin MT, et al. Mitochondrial transfer from bone-marrow-derived stromal cells to pulmonary alveoli protects against acute lung injury. *Nat Med*. 2012;18:759–765.
48. Liu K, Ji K, Guo L, et al. Mesenchymal stem cells rescue injured endothelial cells in an in vitro ischemia-reperfusion model via tunneling nanotube like structure-mediated mitochondrial transfer. *Microvasc Res*. 2014;92:10–18.
49. Hanna SJ, McCoy-Simandle K, Leung E, Genna A, Condeelis J, Cox D. Tunneling nanotubes, a novel mode of tumor cell-macrophage communication in tumor cell invasion. *J Cell Sci* 2019;132:jcs223321.
50. Aga M, Bradley JM, Keller KE, Kelley MJ, Acott TS. Specialized podosome- or invadopodia-like structures (PILS) for focal trabecular meshwork extracellular matrix turnover. *Invest Ophthalmol Vis Sci*. 2008;49:5353–5365.
51. He K, Sakai T, Tsukasaki Y, Watanabe TM, Ikebe M. Myosin X is recruited to nascent focal adhesions at the leading edge and induces multi-cycle filopodial elongation. *Sci Rep*. 2017;7: 13685.
52. Chugh P, Paluch EK. The actin cortex at a glance. *J Cell Sci*. 2018; 131.
53. Gonzalez JM, Ko MK, Pouw A, Tan JC. Tissue-based multiphoton analysis of actomyosin and structural responses in human trabecular meshwork. *Sci Rep*. 2016;6:21315.
54. Bovellan M, Romeo Y, Biro M, et al. Cellular control of cortical actin nucleation. *Curr Biol*. 2014;24:1628–1635.
55. Delage E, Cervantes DC, Penard E, et al. Differential identity of Filopodia and tunneling nanotubes revealed by the opposite functions of actin regulatory complexes. *Sci Rep*. 2016;6:39632.
56. Schiller C, Diakopoulos KN, Rohwedder I, et al. LST1 promotes the assembly of a molecular machinery responsible for tunneling nanotube formation. *J Cell Sci*. 2013;126:767–777.
57. Onfelt B, Nedvetzki S, Benninger RK, et al. Structurally distinct membrane nanotubes between human macrophages support long-distance vesicular traffic or surfing of bacteria. *J Immunol*. 2006;177:8476–8483.
58. Linder S, Kopp P. Podosomes at a glance. *J Cell Sci*. 2005;118: 2079–2082.

Supplementary Material

Supplementary Video S1. Live-cell imaging of the actin cytoskeleton in NTM cells. Actin was labeled with SiR-actin and cells were imaged every 2 minutes for 2 hours. The videos were made at three frames per second.

Supplementary Video S2. Live-cell imaging of the actin cytoskeleton in GTM cells. Actin was labeled with SiR-actin and cells were imaged every 2 minutes for 2 hours. The videos were made at three frames per second.

Investigative Ophthalmology & Visual Science